A spatio-temporally compensated acousto-optic scanner for two-photon microscopy providing large field of view

Y. Kremer, J.-F. Léger, R. Lapole, N. Honnorat, Y. Candela, S. Dieudonné, Laurent Bourdieu

A spatio-temporally compensated acousto-optic scanner for two-photon microscopy providing large field of view.

Y. Kremer, J.-F. Léger, R. Lapole, N. Honnorat, Y. Candela, S. Dieudonné and L. Bourdieu*

Laboratoire de Neurobiologie, Ecole Normale Supérieure, CNRS, 46 rue d'Ulm, 75005 Paris
** Corresponding author: laurent.bourdieu@ens.fr*

Abstract: Acousto-optic deflectors (AOD) are promising ultrafast scanners for non-linear microscopy. Their use has been limited until now by their small scanning range and by the spatial and temporal dispersions of the laser beam going through the deflectors. We show that the use of AOD of large aperture (13mm) compared to standard deflectors allows accessing much larger field of view while minimizing spatio-temporal distortions. An acousto-optic modulator (AOM) placed at distance of the AOD is used to compensate spatial and temporal dispersions. Fine tuning of the AOM-AOD setup using a frequency-resolved optical gating (GRENOUILLE) allows elimination of pulse front tilt whereas spatial chirp is minimized thanks to the large aperture AOD.

OCIS codes: (180.4315) Nonlinear microscopy; (180.5810) Scanning microscopy; (230.1040) Acousto-optical devices.

References and Links

1. D. Li, X. Lv, S. Zeng, and Q. Luo, "Beam spot size evolution of Gaussian femtosecond pulses after angular dispersion," Opt. Lett. **33**, 128-130 (2008).
2. D. R. Li, X. H. Lv, S. Q. Zeng, and Q. M. Luo, "A generalized analysis of femtosecond laser pulse broadening after angular dispersion," Opt. Express **16**, 237-247 (2008).
3. D. R. Li, S. Q. Zeng, X. H. Lv, J. Liu, R. Du, R. H. Jiang, W. R. Chen, and Q. M. Luo, "Dispersion characteristics of acousto-optic deflector for scanning Gaussian laser beam of femtosecond pulses," Opt. Express **15**, 4726-4734 (2007).
4. S. Zeng, D. Li, X. Lv, J. Liu, and Q. Luo, "Pulse broadening of the femtosecond pulses in a Gaussian beam passing an angular disperser," Opt. Lett. **32**, 1180-1182 (2007).
5. J. D. Lechleiter, D. T. Lin, and I. Sieneart, "Multi-photon laser scanning microscopy using an acoustic optical deflector," Biophys. J. **83**, 2292-2299 (2002).
6. R. D. Roorda, T. M. Hohl, R. Toledo-Crow, and G. Miesenbock, "Video-rate nonlinear microscopy of neuronal membrane dynamics with genetically encoded probes," J. Neurophysiol. **92**, 609-621 (2004).
7. V. Iyer, B. E. Losavio, and P. Saggau, "Compensation of spatial and temporal dispersion for acousto-optic multiphoton laser-scanning microscopy," J. Biomed. Opt. **8**, 460-471 (2003).
8. Ngoi, "Angular dispersion compensation for acousto-optic devices used for ultrashort-pulsed laser micromachining," Opt. Express **9**, 200-206 (2001).
9. R. Salome, Y. Kremer, S. Dieudonne, J. F. Leger, O. Krichevsky, C. Wyart, D. Chatenay, and L. Bourdieu, "Ultrafast random-access scanning in two-photon microscopy using acousto-optic deflectors," J. Neurosci. Methods **154**, 161-174 (2006).
10. M. Fork, Gordon, "Negative dispersion using pairs of prisms," Opt. Lett. **9**, 150-152 (1984).
11. S. Zeng, X. Lv, C. Zhan, W. R. Chen, W. Xiong, S. L. Jacques, and Q. Luo, "Simultaneous compensation for spatial and temporal dispersion of acousto-optical deflectors for two-dimensional scanning with a single prism," Opt. Lett. **31**, 1091-1093 (2006).
12. S. Zeng, K. Bi, S. Xue, Y. Liu, X. Lv, and Q. Luo, "Acousto-optic modulator system for femtosecond laser pulses," Rev. Sci. Instrum. **78**, 015103 (2007).
13. S. Zeng, X. Lv, K. Bi, C. Zhan, D. Li, W. R. Chen, W. Xiong, S. L. Jacques, and Q. Luo, "Analysis of the dispersion compensation of acousto-optic deflectors used for multiphoton imaging," J. Biomed. Opt. **12**, 024015 (2007).
14. X. Gu, S. Akturk, and R. Trebino, "Spatial chirp in ultrafast optics," Opt. Commun. **242**, 599-604 (2004).

15. S. Akturk, X. Gu, E. Zeek, and R. Trebino, "Pulse-front tilt caused by spatial and temporal chirp," Opt. Express **12**, 4399-4410 (2004).
16. M. Nakazawa, T. Nakashima, and H. Kubota, "Optical pulse compression using a TeO2 acousto-optical light deflector.," Opt. Lett. **13**, 120-122 (1988).
17. S. Akturk, M. Kimmel, P. O'Shea, and R. Trebino, "Measuring pulse-front tilt in ultrashort pulses using GRENOUILLE," Opt. Express **11**, 491-501 (2003).
18. S. Akturk, M. Kimmel, P. O'Shea, and R. Trebino, "Measuring spatial chirp in ultrashort pulses using single-shot Frequency-Resolved Optical Gating," Opt. Express **11**, 68-78 (2003).
19. S. Akturk, X. Gu, P. Gabolde, and R. Trebino, "The general theory of first-order spatio-temporal distortions of Gaussian pulses and beams," Opt. Express **13**, 8642-8661 (2005).

1. Introduction

Two-photon scanning microscopy (TPSM) is a powerful tool for imaging deep inside living tissues with sub-cellular resolution. The spatio-temporal resolution of currently available TPSM is strongly limited by the galvanometric mirrors which scan the laser beam. Full images at frame rates of 10 to 100 Hz have been obtained, but events occurring at a ms timescale can only be followed by scanning repeatedly a single line. This approach severely constrains the spatial sampling. Because acousto-optic deflectors (AOD) are non-mechanical devices, they allow access at any angle within a few microseconds. Fast point by point scanning strategy using AOD might for this reason increase both the signal-to-noise ratio and the sampling rate with respect to galvanometric full frame imaging, since more time is spent on each point of interest. However, the use of AOD with femtosecond pulses is not straightforward and an accurate description of pulse width and laser beam spot evolution after such an angular dispersive element was only recently proposed [1-4]. Many issues have indeed to be overcome in order to implement AOD as standard scanners in TPSM.

First, large spatio-temporal distortions of the femtosecond pulses are introduced by the AOD due to the propagation and the diffraction in the deflectors. These complex distortions need to be measured and compensated to use AOD in two-photon microscopy. Many recent papers have measured and compensated the angular and the temporal dispersions separately. An additional dispersive element placed before the AOD was used to create a spatial dispersion of same magnitude but opposite sign than the one due to the AOD at the center of the field of view (FOV): e.g. a prism [5, 6], a diffraction grating [7] or an acousto-optic modulator (AOM) [8, 9]. Compensation of temporal dispersion was usually obtained through double pass within a pair of prisms or gratings [10]. The large group delay dispersion (GDD) introduced by TeO_2 which our AOD are made of, requires inter-prism distance of the order of 1m, which induces constraints on the space, the optical alignment and therefore on the possibility to implement research and commercial prototypes.

AOD and setups for temporal and spatial compensation are also introducing large power loss. Two crossed TeO_2 AOD in shear mode have typically a transmission of 50%, spatial compensation setups (AOM or prism) 70 to 80%, and temporal compensation setup consisting of a double pass in a pair of prisms about 70%. Taking into account typical transmission of the rest of the microscope including the objective, the remaining available power at the sample might only be 5 to 10 % of the initial power and therefore strongly limits the depth of imaging *in vivo*. Recent studies have shown that placing the dispersive element (AOM or prism) used for spatial compensation at a distance of the AOD can simultaneously create the appropriate negative dispersion [11-13]. This configuration allows minimization of laser power loss and facilitates optical alignment. However such a single pass in a pair of angular dispersive elements is known to create spatial distortions, as e.g. spatial chirp (SC) [14]. In absence of geometrical aberrations and in a neither scattering nor absorbing sample, SC is in principle suppressed at the focal point of the objective. The situation is more complex in scattering samples or in presence of e.g. spherical aberrations. As the path of border wavelengths will be different from the one of central wavelengths, scattering and/or aberrations might contribute to an increase of the pulse duration at the focal point, thus reducing fluorescence excitation in an uncontrolled manner. Finally, misalignment of such angular dispersive systems as well as propagation of pulses having spatial chirp through

optical windows can also generate pulse front tilt (PFT) [15]. It is therefore important to carefully characterize and minimize the SC and PFT created by the AOM–AOD scanner.

Moreover, the number of points N scanned with an AOD (and therefore the available FOV) is limited by their physical dimension and their maximal scan angle $\Delta\theta$ ($N=(\pi/4)\ \Delta\theta\ D/\lambda$). Most systems used in the literature have a scanning range $\Delta\theta$~40mrad and a physical dimension of a few millimeters (typically 4mm) corresponding to ~ 200 points per line. As a consequence, the FOV has to be smaller than about 100µm in order to have a diffraction limited point spread function (PSF) at the center of the field of view (~0.5µm). Larger FOV are only achievable using AOD with larger scanning angle and/or aperture. Finally, the widespread use of AOD as scanners in TPSM requires that they might be used with tunable lasers over a large bandwidth [12]. This implies to design AOD as well as compensation setups that are efficiently tunable over similar bandwidths.

In this letter, we fully characterize a custom made AOD scanner from the company A&A having exceptional physical dimensions and performance: 13mm aperture, 50mrad scanning range, a tuning range of 720-880nm allowing access to about 850 points per line (7.10^5 points in the FOV). Spatial and temporal compensations are obtained using an AOM placed at distance of the AOD. Using a GRENOUILLE, an easy to align Frequency-Resolved Optical Gating (FROG), i.e. a spectrally resolved auto-correlator, we show that temporal broadening and spatial dispersion can be minimized using this setup. Moreover, we have characterized the spatio-temporal distortions including spatial chirp and pulse front tilt which arise from the single pass in the AOM-AOD setup. We demonstrate that the fine tuning of the AOM-AOD setup and the use of large aperture AOD allow minimization of PFT and SC.

2. Experimental methods

The setup (Fig. 1) consisted of a Tsunami Ti:sapphire femtosecond laser source (Spectra Physics, Irvine, CA) which provided ~ 90fs pulses having a spectrum $\delta\lambda$ ~11+/- 0.5nm (FWHM). The beam was magnified by a first afocal telescope (magnification ~ 8) to a beam diameter D_0 of about 11mm (measured at $1/e^2$), which slightly under-covered the AOM aperture (13mm, ref AA.MTS/A15@720-920nm, A&A, Orsay, France). The AOD pair (A&A, ref AA.DTS.XY/A15@720-920nm) was placed at a distance D of the AOM. D was about 60cm and was carefully adjusted for optimal temporal compensation. The AOD aperture (13mm) was chosen so that it didn't diaphragm the laser beam, despite its spectral divergence after the AOM. A $\lambda/2$ achromatic waveplate was placed between the AOM and the AOD to adjust the pulse polarization. The AOD exit aperture was imaged by a telescope of magnification 1/3 onto a spectrally resolved auto-correlator (GRENOUILLE 10-50, Swamp Optics, Atlanta). A second $\lambda/2$ achromatic waveplate was used for convenience to adjust the light polarization. QuickFrog software (version 3.1, Swamp optics) was used to reconstruct the electric field from the measurement. A glass slide placed after the AOD was used to collect a small fraction of the beam which was focalized onto a digital CDD camera (IMI-141-FT, IMI tech, Seoul, Korea) using a f=75mm lens to measure the spatial dispersion of the pulses and to optimize its compensation. The ultrasonic wave frequency and amplitude were controlled in the AOM using a AA.MOD-nC driver (A&A) with a remote control and in the AOD using a DDS-XY-70-140-D8b-3W driver (A&A) and a program written with Labview using a fast digital I/O board (NI PCI DIO 32HS, National Instruments). This large AOM-AOD device will be referred to as *scanner 1* in the following.

For comparison, a second scanning system was used. It consists of an AOM (AA.MTS.141/B20/A5@840nm, A&A) and 2 crossed AOD (AA.DTS.XY.250@840nm, A&A) optimized at a wavelength of 840nm, having a smaller aperture of 4.2mm and driven by AA.MOD-nC (A&A) and AA.DDS.1-250.2V (A&A) drivers respectively. In that case, a beam diameter D_0~3mm was used at the AOM entrance pupil. This small AOM-AOD setup will be referred to as *scanner 2* in the following. It was used with a Mai-Tai Ti:Saphire laser (Spectra Physics), with a spectrum of $\delta\lambda$ ~14+/- 0.5nm (FWHM).

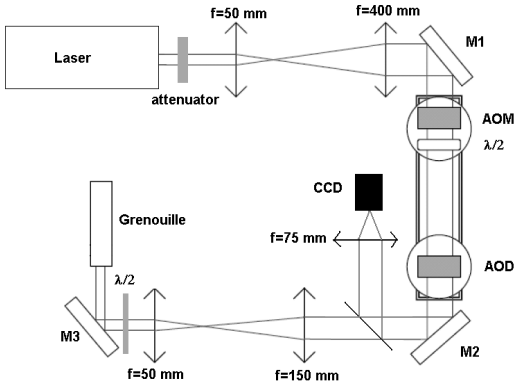

Fig. 1. The optical setup. Laser: Tsunami Ti:Sa laser. AOM: acousto-optic modulator and AOD: acousto-optic deflectors. Both were mounted on goniometric plates for alignment and placed on a rail to adjust their distance. λ/2: achromatic half waveplates. GRENOUILLE: single shot second harmonic generation frequency-resolved optical gating devices. M1, M2, M3: dielectric mirrors. Attenuator: variable intensity attenuator.

3. Background

3.1 Spatial dispersion

In acousto-optic devices used in the Bragg mode, light is efficiently deflected into the first diffraction order at an angle θ given by:

$$\theta = \lambda.F/v \tag{1}$$

where λ is the wavelength of the light, F (~100MHz) the acoustic frequency and v (~650m/s) the velocity of the acoustic wave inside the crystal. AOD are working at a central frequency F_0 over a bandwidth $+/-\Delta F/2$, of the order of 15 to 20 MHz. The maximum scan angle $\Delta\theta$ is therefore given by $\Delta\theta = \lambda.\Delta F/v$~40mrad. Femtosecond lasers required for non-linear fluorescence absorption have a broad spectrum $\delta\lambda \sim$ 10-15nm. The spectral components are therefore spatially dispersed by an AOD over an angle $\delta\theta$ given:

$$\delta\theta/\theta=\delta\lambda/\lambda \tag{2}$$

As $\delta\theta$ is of the order of 1.5 to 2.5mrad, this effect increases the point spread function (PSF) of the microscope (therefore reducing its spatial resolution) and decreases the non-linear fluorescence absorption and strongly constrains the size of the FOV [9]. With two crossed AOD, the result of this angular dispersion is an elliptical PSF [9].

3.2 Temporal dispersion

AOD are made of a material which broadens the pulse duration, since TeO_2 is highly dispersive with large group velocity dispersion *GVD*. In the AOD, the pulse travels a length l_e along the extraordinary axis (*GVD* along the extraordinary axis (GVD_e) of 4840 fs^2/cm at 840nm) and a length l_o along the ordinary axis (*GVD* along the ordinary axis (GVD_o) of 4720 fs^2/cm at 840nm), with $l_e+l_o=L$, where L is the AOD thickness. As a consequence, a transform-limited laser pulse with a Gaussian envelope and of initial duration t_{in} is broadened, by the AOD to a final duration t_{out}, given by:

$$t_{out} = t_{in}.\sqrt{1+\left(4.\ln 2.(l_e.GVD_e + l_o GVD_o)/t_{in}^2\right)^2} \tag{3}$$

Typically, pulses are broadened to at least 500fs using standard AOD [7, 9, 13].

3.2 Compensation of spatial dispersion

It is possible to place an AOM just before the AOD at an angle of 45° with respect to the AOD axes, in order to compensate the spatial dispersion at the centre of the FOV [9]. The frequency in the AOM is then chosen equal to:

$$F_{AOM} = \sqrt{2}.F_0 \tag{4}$$

where F_0 is the frequency at the centre of the FOV in both AOD. The AOM behaves like a prism of adjustable apex, so that F_{AOM} can be finely tuned to optimize the compensation. Moreover, an AOM provides a very high transmission above 80%. The angular dispersion is totally compensated at the centre of FOV and partially at the edge, the maximum remaining dispersion being proportional to $\Delta F/2$ instead of F_0 [9]. For frequencies in the AOD $F=(Fx,Fy)$, the corresponding ellipse has a long axis w^l, a small axis w^s and an ellipticity e given by [9]:

$$w^l = \sqrt{w_r^2 + \left(\frac{\delta\lambda(|F - F_0|) f_{obj}}{vT}\right)^2} \;,\; w^s = w_r \;;\; e = \frac{w_l}{w_s} \tag{5}$$

where w_r is the radial resolution of the microscope in absence of AOD, defined as the FWHM of the squared intensity point spread function (IPSF^2), f_{obj} is the objective focal length, T is the magnification of the telescope used to image the AOD onto the objective back aperture and $\Delta F = |F - F_0| = \sqrt{(F_x - F_0)^2 + (F_y - F_0)^2} = \sqrt{\Delta F_x{}^2 + \Delta F_y{}^2}$. The ellipse angle ϕ is given by:

$$\tan\varphi = \Delta F_y / \Delta F_x \tag{6}$$

3.3 Simultaneous compensation of temporal and spatial dispersion

Negative GDD can be obtained from devices providing angular dispersion such as prisms or gratings. Most standard pre-compensation setups consist of a double pass through a pair of prisms [10] and were used to compensate for the positive GDD introduced by AOD. Nakazawa and al. have shown that pairs of AOD provide also negative GVD proportional to their distance [16]. For a pair of AOD (or for an AOM AOD setup) separated by a distance D and characterized by their frequencies F, the sound velocity v and the total material thickness L, the group delay dispersion is equal to:

$$GDD_{AOD-AOD} = GDD_{AOD} + D.GVD_{AOD/AOD} \tag{7a}$$

$$GDD_{AOD} == \frac{\lambda^3}{2\pi c^2} L \frac{d^2 n}{d\lambda^2} \tag{7b}$$

$$GVD_{AOD/AOD} == -D \frac{\lambda^3}{2\pi c^2} \frac{F^2}{v^2} \tag{7c}$$

GDD_{AOD} is the positive GDD introduced by the material which the AOD and the AOM are made of and $GVD_{AOD/AOD}$ is negative and proportional to the distance D.

Therefore, as previously described by Zeng et al. [11-13], placing an AOM at a distance D of the AOD allows the compensation of both the temporal and the spatial dispersion at the same time with a single setup and using independent control parameters: temporal compensation is controlled by the distance D whereas spatial compensation is adjusted by the AOM frequency f_{AOM}.

3.4 Spatio-temporal distortions: spatial chirp and pulse front tilt

Since this configuration provides a single path trough the two dispersing AOD, fs pulses might contain spatio-temporal distortion, in particular spatial chirp (SC), in which the average wavelength of the pulse varies spatially across the beam [14]. In our case, the spatial chirp is described by the beam centre transverse coordinate x of each frequency ω [14]. A pulse passing through an AOM placed at a distance D of the AOD has a dispersion $x(\omega) \approx D\theta = D\,2\pi cF/\omega v$. The scanner is imaged onto the GRENOUILLE (or the objective back aperture) by a telescope (magnification $T \sim D_a/D_0$ to match their aperture D_a). The spatial dispersion at their aperture is $x_a(\omega) \approx D(2\pi c/\omega)(F/v)(D_a/D_0)$ and the spatial chirp $\zeta_a = dx_a/d\omega = \dfrac{D2\pi cFD_a}{v\omega^2 D_0} = \dfrac{DF\lambda^2 D_a}{v2\pi cD_0}$. The amount of spatial chirp can be estimated by comparing the characteristic length $\zeta_a.\Delta\omega$ (where $\Delta\omega = 2\pi c\,\delta\lambda/\lambda^2$) and the beam diameter D_a:

$$R = \zeta_a.\Delta\omega/D_a = DF\delta\lambda/vD_0. \quad (8)$$

Equation 8 shows that the spatial chirp increases with the distance D between the AOM and the AOD and decreases with the beam diameter D_0 at the scanner aperture. At the typical distance used for temporal compensation ($D \sim 50$cm), $R \sim 1.3\text{mm}/D_0$ and deflectors having an aperture smaller or of the order of 1.3mm will induce strong SC in the pulse, whereas SC will vanish for scanners much larger than this dimension.

Angular dispersion as well as propagation of a pulse having some SC through a material induce also some pulse front tilt (PFT) [15, 17], which consists in the fact that the time at which the pulses reach a plane of reference depends on the transverse coordinate x. PFT increases the pulse duration at the objective focal point. Since a single path through the AOM-AOD setup potentially creates spatio-temporal distortions as PFT and SC, it is important to measure them carefully. Both SC and PFT are easily measured by a single shot second harmonic generation frequency-resolved optical gating devices. Thus we characterized these distortions using a spectrally resolved auto-correlator, as a GRENOUILLE, which is sensitive to PFT and to a lesser extent to SC.

4. Experimental results

4.1 Spatial compensation

Figure 2(a) shows, for three different wavelengths, typical scans of the field of view on the CCD achieved with the large aperture scanner 1. By adjusting properly the AOM frequency in each case, full spatial compensation was achieved at the centre of the *FOV*. Elsewhere, the laser was focalized as ellipses, which are all oriented towards the centre and which increase in size towards the edges of the image. Whereas their small axis is constant in the *FOV*, their long axis increases with the distance to the centre. On Fig. 2(b), we measured at 820nm their ellipticity as a function of the shift in frequency with respect to the centre frequency, which is perfectly modeled by Eq. (5). Similarly, their angle was measured on Fig. 2(b) as a function of the frequency ratio $\Delta F_y/\Delta F_x$. and modeled with Eq.6.

These results are consistent with previous results obtained with small aperture scanners [7, 9, 11, 13]. We show similarly on Fig. 2(b) that compensation of spatial dispersion of scanner 2 is achieved at 840nm and modeled perfectly by Eqs.5 and 6, as published previously [9]. The difference in ellipticity measured for the 2 scanners is due, as shown from Eq. (5), from the differences in the focal length of the CCD lens used (in order to match their different scan range) and in beam diameter after the AOD (and therefore in spot diameter at the center of the FOV). For the scanner 2, the optimum frequency in the AOM was equal to 142 MHz, with a central frequency in the AOD of 100MHz, in agreement with Eq. (4) and with a bandwidth of 35MHz (45mrad).

To compensate for the spatial dispersion at different wavelengths in scanner 1, the AOM frequency was changed accordingly, as shown on Fig. 2c. We found that the optimum AOM

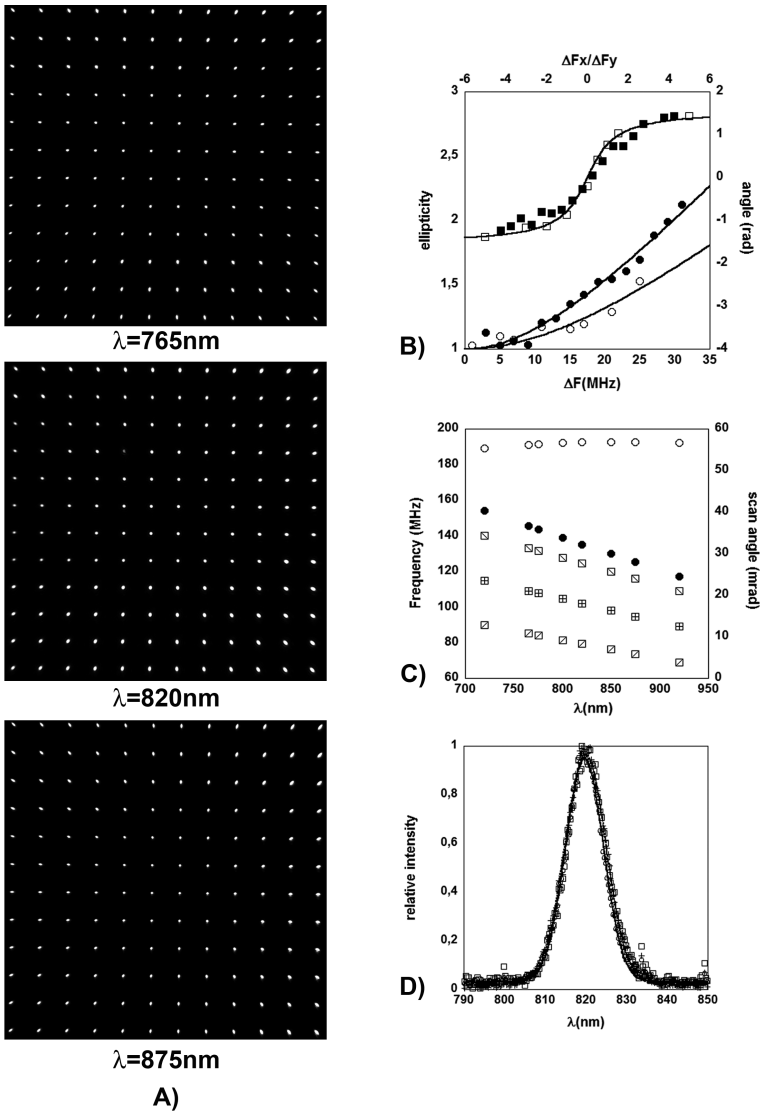

Fig. 2. Compensation of spatial dispersion. A) Images at 765nm, 820nm and 875nm of the beam scanned by the scanner 1 and focused on the CCD. Spots are separated by 3.7mrad. B) Spot ellipticity (●) as a function of ΔF and spot angle (■) as function of $\Delta F_x/\Delta F_y$. Data obtained from images at 820nm containing 14x14 ellipses separated by 3.5 MHz (4.4mrad) were binned (bin for ΔF: 2MHz, bin for $\Delta Fx/\Delta Fy$: 0.5). Lines are the theoretical curves obtained from Eqs.5 and 6 respectively. For comparison, spot ellipticity (○) and spot angle (□) are shown for the small scanner 2 using the same bins. C) AOM frequency (●), AOD minimum (⊡), centre (⊞) and maximum (⧅) frequencies and maximum scan angle (○) as a function of the wavelength for the scanner 1. D) Laser spectrum measured before the AOM (□), between the AOM and the AODs (○) and after the AODs (+) for scanner 1. Data were fitted to Gaussians having the same FWHM=11+/-0.5nm.

frequency was shifted by a small constant offset of 9MHz with respect to the frequency predicted by Eq. (4). This prevented perfect compensation above 880nm, due to the limited bandwidth of our AOM and the scanner was therefore used from 720nm to 880nm. Figure 2(c) shows also the variation of the AOD minimum, maximum and centre frequencies. The

resulting scan angle was constant as a function of the wavelength, of the order of 56mrad. Within the FOV, the laser intensity was varied by less than 20%. Finally, the typical transmission of the AOM-AOD scanner was of the order of 20%.Theses results demonstrate that compensation of the spectral dispersion is achieved at the centre of the *FOV* from 720nm up to 880nm and that the remaining dispersions are well modeled by Eqs. (5) and (6).

We checked that the scanner 1 did not diaphragm the laser beam in this configuration. Due to the spectral dispersion in the AOM, the beam diameter increases after the AOM as $\approx D.\delta\lambda.F/v$ ~1.7mm for D=60cm. Figure 2(d) shows that the laser spectrum is preserved at all locations throughout the optical path (FWHM=11nm), even for the large distance D used for temporal compensation (see below). Therefore, using a beam width of ~11mm at the AOM entrance pupil prevents any clipping in the AOD. For comparison, the standard scanning system 2 required for this reason a beam width of ~ 2.8mm only. The achievable FOV is proportional to the product of the scanning angle and of the beam aperture at the scanner. Therefore our new system (scan angle ~56mrad, beam aperture ~11mm) offers a very significant increase in the available FOV (by a factor of 5) in the configuration where the AOM is placed at distance of the AOD for simultaneous temporal and spatial compensation, as compared to the standard scanning system 2 (45mrad, 2.8mm). For example, using the 20X, NA 0.95, water immersion Olympus objective widely used in two-photon microscopy, a FOV of about 300µm will be obtained, with diffraction limited focalization at the centre of the FOV. On the edge of the FOV, the PSF will be stretched in one direction to about 3.7µm, as estimated using Eq. (5). This effect will reduce the resolution and the fluorescence excitation for objects located on the side of the FOV. While scanning an object larger than the PSF, the loss in fluorescence should be proportional to square of the ellipse elongation [9]. This is still acceptable, in comparison to the gain in scanning speed, as long as resolution isn't a priority. Moreover, more time can be spent on the points located near the edges to obtain a constant fluorescence signal.

4.2 Temporal compensation

At the optimum AOM frequency for spatial compensation, we adjusted the distance D separating AOD and AOM to compensate for the temporal dispersion of the laser pulse. This adjustment did not affect the spatial compensation, both being independent. The pulse duration was measured as a function of the distance D and at 820nm using the GRENOUILLE (Fig. 3(a)). As the distance D was increased, pulse duration decreased remarkably down to a value of 93+/-3fs for D ~ 63+/-3cm and increased again for larger distances. This demonstrates that excellent pulse compensation was achieved, since the initial pulse duration was almost restored. Using the same configuration, we were also able to compensate temporally for the dispersion of the scanner 2 at 840nm (Fig. 3(b)). In that case, optimal compensation was obtained at a shorter distance D, of about 45+/-3cm, although longer pulses (145+/10fs) were obtained in this case. This might be due to the fact we used pulses with larger FWHM with this scanner (14nm instead of 11nm). Using Eq. (7), the negative dispersion introduced by the AOM-AOD setup is ~ 460fs^2/cm for the scanner 1 at 820nm and ~ 490fs^2/cm for the scanner 2 at 840nm. Using these values, the scanner 1 has a total *GDD* ~ 29000 fs^2 and the scanner 2 ~22000fs^2. Taking into account known values of the ordinary (GVD_o) and extraordinary (GVD_e) group velocity dispersion of TeO_2 [9] and the physical size of the scanners, we estimated their *GDD*. For the large scanner 1, we obtained a *GDD* at 820nm of ~ 29500 fs^2 (total thickness for each AOD and for the AOM of the scanner 20mm, 10mm interaction with GVD_o~4952fs^2/cm and 10mm interaction with GVD_e~5070fs^2/cm). For the small scanner 2, we estimated at 840nm the *GDD* to be 21300fs^2 (total thickness for each element 15mm, 4mm interaction with GVD_e=4840fs^2/cm, 11mm interaction with GVD_o=4720fs^2/cm). Both values are in good agreement with the values deduced from the experiments.

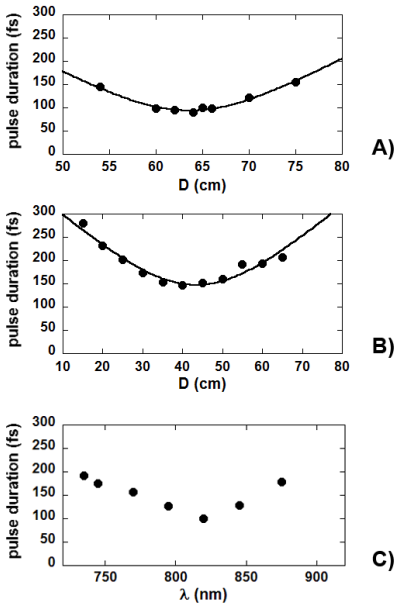

Fig. 3. Temporal compensation. Pulse duration (fs) as a function of the AOM-AOD distance (D) measured: A) at 820 nm for the large scanner 1; B) at 840 nm for the small scanner 2. The lines are fit to the data using Eq.3. C) Pulse duration (fs) measured as a function of the wavelength λ (nm) for the scanner 1 (D=63cm).

We measured for the large scanner 1 by how much the pulse duration varied when the wavelength was changed. Optimal pulse compensation was obtained at different distances *D* depending on the wavelength and typically varied by 10cm for a 50nm change in wavelength. Experimentally, it is hardly possible to vary *D* rapidly during an experiment, since AOD have to be aligned precisely to obtain maximum diffraction efficiency. A more practical configuration was obtained by keeping the distance *D* fixed while varying the wavelength (Fig. 3(c)). In this case, the pulse duration varied from 93fs to 195fs over the scanner bandwidth (720nm - 870nm). Such pulse durations are still very convenient for most two photon microscopy experiments.

4.3 Pulse front tilt and spatial chirp

GRENOUILLE traces allow us to give an estimation of the spatio-temporal distortions of the pulse. Spatial chirp is evidenced as a non-symmetrical trace with respect to the wavelength axis, whereas pulse front tilt is shown by a shift of the trace along the delay axis [15, 17-19]. Figure 4 shows the GRENOUILLE traces obtained with the two AOD systems at different distances *D*. In the case of the large scanner 1, the shape of the GRENOUILLE traces were symmetrical with respect to the vertical axis, whatever the distance D (Fig. 4a). In the case of the smaller scanner 2, a shear was clearly observed for D=75cm (Fig. 4(b), D=75cm). The comparison between the two GRENOUILLE traces demonstrates that spatial chirp was specifically present in the case of the small scanner, as expected from Eq. (8). Moreover, this effect was clearly evidenced at larger distances *D*, as shown from Eq. (8), typically above ~ 50cm. In opposition, for the scanner 1, no spatial chirp was evidenced by the GRENOUILLE whatever the distance *D*. This can be attributed to the fact that the dimension of the beam used with the scanner 1 was very large, and therefore the ratio given by Eq. (8) and characterizing the importance of SC remains small at all distances.

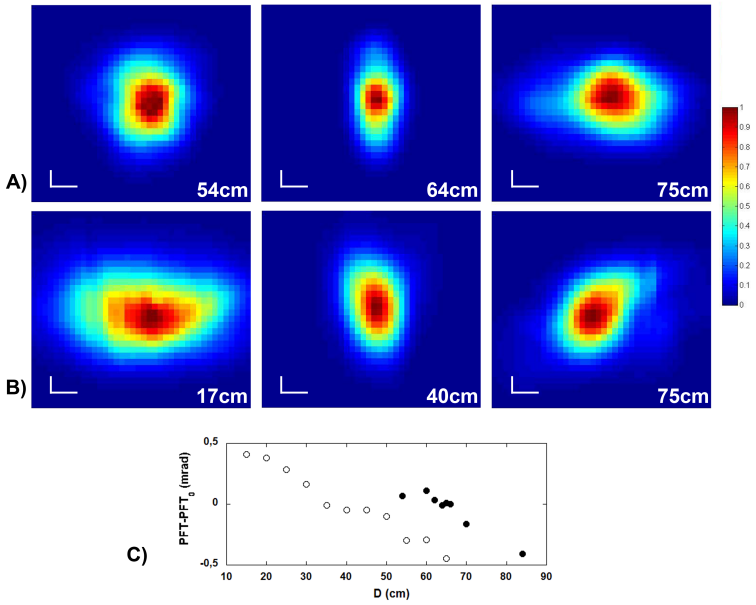

Fig. 4. Spatio-temporal distortions. GRENOUILLE traces measured for 3 AOM-AOD distances: A) for the scanner 1 (D=54cm, D=64cm and D=75cm) B) for the scanner 2 (D=17cm, D=40cm and D=75cm). C) Pulse front tilt as a function of the distance D for the scanner 1 (●) and for the scanner 2 (○). Horizontal bar: 100fs, vertical bar: 1nm.

GRENOUILLE also allows us to estimate the PFT as a function of the distance *D*. Figure 4c shows that the PFT decreases as function of *D* from a positive to a negative value and reaches a value close to 0 at the distance where the pulse duration was minimum. At that distance, for both scanners, a residual PFT was often found (of the order of ~ 0 to 10^{-4}rad) and was very sensitive to the alignment of the setup. Therefore the GRENOUILLE allows control and minimization of the PFT due to the AOM-AOD scanner.

5. Discussion

In the recent years, many groups have designed two-photon microscopes incorporating AOD scanners and have tried to compensate for spatial and temporal dispersions by different methods including additional optics as prisms, gratings or AOM. First setups were using separate devices for both compensations, whereas it has been shown recently that a single prism or AOM placed at the correct distance of the AOD could correct both simultaneously. However, these compact and easier to align setups were not characterized in terms of spatio-temporal distortions (SC and PFT) which are inherent to a single pass in two refracting devices and might occur in misaligned systems. Since AOD alignment is delicate in this configuration and since SC and PFT might affect two-photon fluorescence excitation, it is important to characterize them properly. Moreover, a severe limitation of AOD is the FOV which can be achieved since their physical dimension is limited in standard systems (4mm in most publications), for a scanning range of about 40mrad. This aperture is even more limited if the AOM is placed at distance to the AOD for simultaneous compensation of temporal dispersion. This paper shows that very large aperture AOD might be used in two-photon microscopy without introducing spatio-temporal distortions and providing very large *FOV*.

We have shown that a 13mm aperture AOD offering potentially a *FOV* of typically 300µm using a 20X objective can be used over a bandwidth of 160nm. Spatial compensation at all wavelengths is achieved using an AOM of identical aperture, whereas temporal dispersion compensation is obtained at an AOM–AOD distance of 63cm. This distance is in agreement with the expected value of the GDD introduced by AOD knowing their physical dimension

and the GVD of TeO_2. We obtained an excellent temporal compensation which allows using an almost fully compensated pulse in a two-photon microscope.

Finally, these large AOD limit the SC introduced by the single pass configuration. Spatial chirp is due to the spatial separation of the pulse wavelengths after the AOD relative to the beam diameter. Since AOD scanners whatever their size introduce the same angular dispersion and since temporal compensation is obtained at distances of same order of magnitude, the use of larger AOD minimizes SC. This might be a great advantage compared to smaller systems where SC will eventually lead to temporal pulse broadening in scattering or aberrant media. E.g. in non-linear microscopy, high numerical aperture objectives are used to image deep in highly scattering medium. In presence of SC, the different frequencies of the pulse travel different path lengths in the tissue. As a result of scattering, the pulse at the objective focus might contain fewer frequencies as expected, thus increasing the pulse width. Finally, the use of the GRENOUILLE allows also finely minimizing the PFT so that it almost vanishes at the distance which compensates for the temporal dispersion. Our experience shows indeed that PFT is often encountered when the AOM AOD scanner is not properly aligned with a GRENOUILLE.

Acknowledgments

This work has been supported by Convention E. 1762 de la Région Ile de France, a « Human Frontier Science Foundation » research grant n°RPG0060/2003-C102, by the French « Ministère de la Recherche et de l'Enseignement Supérieure » (ANR Blanche 2007 n°06-BLAN-0178-02), the SDV department of CNRS (ATIP jeune chercheur 2005), and the « ministère de la recherche » of Luxembourg. We thank Manuel Joffre for several useful comments, Benjamin Mathieu for his help in software programming and Rick Trebino for his advices on the use of the GRENOUILLE.